γ-irradiation generated ferrous ions affect the formation of magnetite and feroxyhyte

I. Marić[1], M. Gotić[2,3], G. Štefanić[2,3], A. Pustak[1], T. Jurkin[1,*]

[1]*Radiation Chemistry and Dosimetry Laboratory, Ruđer Bošković Institute, Bijenička c. 54,10000 Zagreb, Croatia*
[2]*Center of Excellence for Advanced Materials and Sensing Devices, Ruđer Bošković Institute, Bijenička c. 54, 10000 Zagreb, Croatia*
[3]*Laboratory for Molecular Physics and Synthesis of New Materials, Division of Materials Physics, Ruđer Bošković Institute, Bijenička c. 54, 10000 Zagreb, Croatia*

Abstract

1,10-phenanthroline spectrophotometric method was used in order to systematically measure the quantity of Fe^{2+} ions that were generated upon γ-irradiation of alkaline Fe(III) aqueous solutions in the presence of diethylaminoethyl (DEAE)-dextran. γ-irradiation was performed in a range of doses from 5 to 130 kGy and the dose rate was ~26 kGy h^{-1}. The results showed that γ-irradiation reduces Fe^{3+} to Fe^{2+}; the reduction was initially very fast, but quickly slowed down and then reached a plateau of 100 % reduction. The quantity of Fe^{2+} in γ-irradiated suspensions and isolated solid products roughly overlap up to 45 % of Fe^{2+}, because in this range the inverse spinel structure of substoichiometric magnetite nanoparticles was able to capture 30.1 % of Fe^{2+}. The stoichiometries of the formed magnetite nanoparticles were very similar, which indicated that the absorbed dose did not have a significant influence on the magnetite stoichiometry, even though Fe^{2+} molar fraction increased from 22 to 45 % as a function of absorbed dose. When γ-irradiation generated 69 % or more of Fe^{2+} the powder samples consisted exclusively of Fe(III), *i.e.* of δ-FeOOH nanodiscs and poorly crystallized α-FeOOH nanoparticles about 4 nm in size. The volume-averaged domain sizes and crystal aspect ratio of the δ-FeOOH nanodiscs increased from 16 nm to 25 nm and from 1.6 to 2.1 with the increase of absorbed dose, respectively. The use of DEAE-dextran in the γ-irradiation synthesis enabled the generation of up to 100 % of Fe^{2+} and synthesis of extremely stable aqueous suspensions of superparamagnetic magnetite nanoparticles as well as the synthesis of δ-FeOOH nanodiscs with high aspect ratios.

Keywords: magnetite; feroxyhyte; gamma-irradiation; DEAE-dextran; 1,10-phenanthroline

*Corresponding author: Dr. Tanja Jurkin, Radiation Chemistry and Dosimetry Laboratory, Ruđer Bošković Institute, Bijenička 54, 10000 Zagreb,
Croatia, Phone: +385 1 4571 255, *E-mail address*: tjurkin@irb.hr

1. Introduction

Magnetic iron oxide nanoparticles have found application in wastewater treatment, magnetic hyperthermia and drug delivery (Gupta and Gupta, 2005; Thomas et al., 2009; Xu et al., 2012). Magnetite (Fe_3O_4) and maghemite (γ-Fe_2O_3) are frequently investigated magnetic iron oxides, whereas much less data is available for feroxyhyte (δ-FeOOH), the only iron oxyhydroxide that is magnetic at room temperature. Magnetite (Fe_3O_4, space group Fd-3m) has an inverse spinel structure with O^{2-} forming a face-centered cubic lattice and iron cations occupying interstitial sites. Ideally, stoichiometric magnetite ($^{Tet}Fe^{III}[^{Oct}Fe^{II}Fe^{III}]O_4$) has the ferrous to ferric ratio $Fe^{II}/Fe^{III} = 0.5$, *i.e.* 33.3 % of total iron in stoichiometric magnetite is present as Fe^{II}. Maghemite (γ-Fe_2O_3, space group $P4_132$) can be regarded as fully oxidized magnetite. The oxidation of magnetite to maghemite involves a reduction in the number of Fe atoms per unit cell of 32 oxygen ions, from 24 in magnetite to 21 1/3 in maghemite. Simultaneously, oxygen vacancies form in the crystal structure of maghemite to account for charge balance ($^{Tet}Fe^{III}_{1.00}[^{Oct}Fe^{II}_{0.00}Fe^{III}_{1.67}\square_{0.33}]O_4$). The substoichiometric magnetite $Fe_{3-x}O_4$ has stoichiometry between Fe_3O_4 and γ-Fe_2O_3. Accordingly, *x* can range from zero in stoichiometric magnetite to 1/3 in completely oxidized magnetite ($Fe_{2.67}O_4$). Magnetite and maghemite are ferrimagnetic at room temperature.

δ-FeOOH structure is based on a hexagonal close-packed (hcp) oxygen lattice similar to that of hematite (α-Fe_2O_3) with iron ions distributed over octahedral and tetrahedral sites or over two octahedral sites (Pernet et al., 1984). The oxygen anions are partly replaced by OH and OH_2 and the degree of occupancy of Fe is less than 2/3 similar as it is in hematite. Sestu et al. (2015) proposed the structure for δ-FeOOH based on the structure of the thermodynamically stable iron oxyhydroxide goethite (α-FeOOH). Feroxyhyte behavior is consistent with ferrimagnetism (Pollard and Pankhurst, 1991). Koch et al. (1995) have considered a well-crystallized feroxyhyte as a planar antiferromagnet with magnetic moments along the *c*-axis. A net magnetization in such materials is due to the very small number of layers along the *c*-direction, which causes the formation of ferromagnetic domains and also, due to the presence of spins randomly canted away from the *c*-axis.

The wet-chemistry route to synthesize magnetite NPs most often involves stirring of a solution of iron salts (Fe^{2+} and Fe^{3+}) with an alkaline compound under an inert atmosphere

(Laurent et al., 2008). For instance, the addition of an aqueous solution of ammonia to a solution of $FeCl_2$ and $FeCl_3$ up to pH ~ 9 will yield magnetite (Massart, 1981). Maghemite can be obtained by the oxidation of magnetite, whereas the synthesis of δ-FeOOH involves the precipitation of $Fe(OH)_2$, which is then quickly oxidized with the addition of hydrogen peroxide (H_2O_2) into δ-FeOOH (Gotić et al., 1994). Thus, the synthesis of all three magnetic iron oxides (group name) depends on the concentration of Fe^{2+} (ferrous) ions. For instance, the synthesis of magnetite requires 33.3 % of Fe^{2+} in the precursor suspension. However, in an aqueous suspension, the Fe^{2+} ions quickly oxidize. Vigorous stirring leads to the oxidation of Fe^{2+} to Fe^{3+} due to the dissolution of oxygen and/or frequent contact of Fe^{2+} with oxygen in air. Contrary to the conventional synthesis methods, γ-irradiation synthesis of magnetite starts exclusively from Fe^{3+} precursors thus completely avoiding the use of easily oxidizing Fe^{2+} ions (Ekoko, 2014; Wang et al., 1997; Wang and Xin, 1999). Generally, γ-irradiation (radiolytic) method involves the interaction of high energy γ-photons (1.25 MeV ^{60}Co) with an aqueous phase. The result of this interaction is the ionization of solvent molecules and the production of a variety of radicals (e_{aq}^-, $H^\bullet$, $OH^\bullet$) and molecular products (H_2, H_2O_2). The formed reducing species (e_{aq}^-, $H^\bullet$) can reduce Fe^{3+} and the reducing conditions can be intensified by purging the precursor suspension with nitrogen in order to remove dissolved oxygen and by using 2-propanol as a scavenger of oxidizing species such as hydroxyl radicals ($^\bullet OH$). In a previous work, we have used the γ-irradiation assisted microemulsion synthesis in order to synthesize magnetite NPs (Gotić et al., 2009, 2007a). It has been shown that the γ-irradiated Fe(III) precursor in a microemulsion transformed to substoichiometric magnetite NPs at a certain dose and dose rate. With increasing dose, the stoichiometry of magnetite improved, but at the same time, goethite developed as a second phase so that the overall effect was that a more oxidized product was formed. In order to explain this contradictory result, we presumed that the reduction and oxidation existed as concurrent competitive processes in the γ-irradiated Fe(III) microemulsion. However, our recent results (Jurkin et al., 2016a), where we studied the impact of various polymers on the synthesis of magnetic iron oxides, have shed new light on why, after a certain optimal dose at which magnetite is produced, a further increase in dose produces only more oxidized products. In fact, we have recently, for the first time and completely unexpectedly, synthesized δ-FeOOH (feroxyhyte) nanodiscs using γ-irradiation. The synthesis of δ-FeOOH nanodiscs using γ-irradiation is a big surprise, because δ-FeOOH has never been synthesized starting from Fe(III)

precursor or using γ-irradiation. We have hypothesized that γ-irradiation generated highly reducing conditions that completely reduced the Fe(III) precursor to Fe(II) intermediate products. Besides, we have observed that the white suspension characteristic of $Fe(OH)_2$ was formed, which after coming in contact with the air turned to a green-gray suspension characteristic of Green Rust. In the conventional process of sample isolation, the green-gray stable suspension transformed to magnetic δ-FeOOH reddish powder that consisted exclusively of Fe(III). Therefore, on the basis of isolated Fe(III) products one cannot conclude about the real reducing conditions produced upon γ-irradiation. Obviously, quantitative measurement of Fe^{2+} is of great importance for a better understanding of the relationship between the concentration of γ-irradiation generated Fe^{2+} and the phase composition of the finally isolated products.

There are several methods to determine iron concentration, such as inductively coupled plasma-atomic emission spectroscopy (Qu et al., 2014), atomic absorption spectroscopy (Seeger et al., 2015), permanganate titration (Marić et al., 2019a), and UV-Vis spectrophotometry methods (Sutherland et al., 2016; Yakabuskie et al., 2011). Even though AES and AAS methods have high accuracy and precision, these methods cannot distinguish between Fe^{2+} and Fe^{3+} and generally, they are more time-consuming, expensive, and need qualified personnel to use these methods. In a previous work we used permanganate titration as a simple and non-expensive method (Marić et al., 2019a, 2019b), however, its accuracy and precision is lacking and is subjective due to the visual determination of the titration endpoint. On the other hand, spectrophotometric methods tend to have good accuracy and precision, require less expensive instrumentation and they are generally easy to handle. For spectrophotometric determination of iron, usually a complexing agent is used for the formation of a colored compound between the ligand and Fe^{2+}. In order to determine the total iron concentration (or Fe^{3+}), the present Fe^{3+} in the solution can be reduced by a mild reducing agent. There is a variety of complexing agents used, such as 2,2'bipyridine (Hartmann and Asch, 2018), ferrozine (Viollier et al., 2000) and 1,10-phenanthroline (Jiang et al., 2017; Tamura et al., 1974). Due to its simplicity, accuracy, and reproducibility, herein we employed a modified 1,10-phenanthroline method for the determination of radiolytically generated Fe^{2+} based on the procedure given by Jiang et al. (2017).

In this work, we used the 1,10-phenanthroline method in order to systematically measure the quantity of Fe^{2+} generated upon γ-irradiation of alkaline Fe(III) aqueous solutions in the

presence of DEAE-dextran. The results showed that γ-irradiation reduces Fe^{3+} to Fe^{2+}; the reduction was initially very fast, but quickly slowed down and then reached 100 % reduction. The quantity of Fe^{2+} in γ-irradiated suspensions and isolated solid product roughly overlap up to 45 % of Fe^{2+}, because at this range the inverse spinel structure of stoichiometric formed magnetite NPs was able to capture 33.3 % of Fe^{2+}. At 69 % or more of Fe^{2+} in suspensions, the isolated solid product counterparts consist exclusively of Fe(III), because the Fe(II)-rich solid products in contact with air readily and completely oxidized to Fe(III) products.

2. Materials and methods

2.1 Chemicals

All chemicals were of analytical purity and used as received without further purification. Iron(III) chloride hexahydrate (*Sigma-Aldrich*, puriss. p.a., Reag. Ph. Eur., ≥99%, Cat. No. 31232), iron(II) chloride tetrahydrate (*Merck*, p.a., Cat. No. 1.03861), sodium hydroxide (*Honeywell*, anhydrous, free-flowing, pellets, ACS reagent, ≥97%, Cat. No. 795429), 2-propanol (*Honeywell*, CROMASOLV, for HPLC, ≥99.9%, Cat. No. 34863), sodium acetate (*Merck*, anhydrous for analysis, EMSURE, ACS, Reag. Ph. Eur., Cat. No. 1.06268), acetic acid (*Honeywell*, puriss. p.a., ACS Reagent, Reag. Ph. Eur., ≥99.8%, Cat. No. 33209), L-ascorbic acid (*Sigma-Aldrich*, BioXtra, crystalline, ≥99.0%, Cat. No. A5960), 1,10-phenanthroline monohydrate (*Sigma-Aldrich*, for the spectrophotometric determination, ≥99.0%, Cat. No. 77500), sulphuric acid (*Honeywell*, puriss. p.a., ACS Reagent, Reag. Ph. Eur., for determination of Hg, 95.0-97.0 %, Cat. No. 30743), hydrochloric acid (*Fluka*, for trace analysis, fuming, ≥37 %, Cat. No. 84415) and Milli-Q deionized water were used. Diethylaminoethyl dextran hydrochloride (DEAE-dextran) prepared from dextran of average molecular weight 500,000 was produced by *Sigma-Aldrich*, Cat. No. D9885.

2.2.1 Synthesis of iron oxide nanoparticles

Firstly, the 2M $FeCl_3$ and 1.85 wt% DEAE-dextran hydrochloride aqueous stock solutions were prepared. Then, 880 μL (1.76 mmol) of 2 M $FeCl_3$ and 1540 μL (20.1 mmol) of 2-propanol were added to 100 mL of 1.85 wt% DEAE-dextran hydrochloride aqueous solution. The pH of the prepared solution was adjusted to ~9.1 by slowly adding 2 M NaOH aqueous

solution. The solutions were bubbled for 30 minutes with nitrogen in order to remove the dissolved oxygen (deaerated solution) and then γ-irradiated (without stirring) in a closed glass vial at room temperature using panoramic ^{60}Co source at Radiation Chemistry and Dosimetry Laboratory at the Ruđer Bošković Institute. The dose rate of γ-irradiation was ~26 kGy h^{-1}. The absorbed doses were from 5 kGy to 130 kGy. The samples were isolated by centrifugation using ScanSpeed 2236R high-speed centrifuge. The isolated precipitates were dried under vacuum at room temperature and then characterized as powder samples. The samples are named as S-X, where X represents the absorbed dose (for instance, S-36 is a sample that was γ-irradiated at a dose of 36 kGy). We have used Roman numerals (e.g., Fe(II) or Fe(III) to denote the oxidation state of iron in solid (isolated) samples, whereas Arabic numerals (e.g., Fe^{2+} or Fe^{3+}) were used to denote iron ions completely dissolved in aqueous solutions.

2.2.2 Characterization of samples

X-ray powder diffraction (XRD) patterns were recorded at 20 °C using an APD 2000 X-ray powder diffractometer manufactured by ItalStructures and a Siemens D5000 diffractometer (Cu*K*α radiation). The XRD patterns were recorded over a 5–80 2θ range with 2θ step of 0.025° or 0.05° and a counting time per step of 20 – 107 s. The samples were put on XRD Si zero-background holder in the form of a thin layer. The XRD patterns were analyzed with the software CMPR (Toby, 2005). Rietveld refinement was performed using MAUD software (Lutterotti et al., 2007).

^{57}Fe Mössbauer spectra were recorded at 20 °C in the transmission mode using a standard instrumental configuration by WissEl GmbH (Starnberg, Germany). The ^{57}Co in the rhodium matrix was used as a Mössbauer source. The spectrometer was calibrated at 20 °C using the standard α-Fe foil spectrum. The velocity scale and all the data refer to the metallic α-Fe absorber at 20 °C. The experimentally observed Mössbauer spectra were fitted using the MossWinn program.

The morphology of the samples was evaluated using a field emission scanning electron microscope (FE SEM, model JSM-7000F) manufactured by JEOL Ltd. connected to the EDS/INCA 350 (energy dispersive X-ray analyzer) manufactured by Oxford Instruments.

UV-Vis spectra were collected with a Shimadzu UV/VIS/NIR spectrometer, model UV-3600. The used wavelength range was from 800 to 300 nm.

2.3.1 Preparation of Fe^{2+} and Fe^{3+} standard solutions

All of the solutions were prepared according to a modified procedure by Jiang et al. (2017). Acetate buffer was prepared by weighing 32.8 g of sodium acetate which was quantitatively transferred to a 200 mL flask. In the same flask, 48 mL of acetic acid was pipetted, and the flask was filled to the mark with deionized water. 10 % solution of ascorbic acid was prepared by adding 5 g of ascorbic acid to a 50 mL flask, which was subsequently filled with deionized water to the mark. 0,1 % solution of 1,10-phenanthroline was prepared by weighing 0.1 g of 1,10-phenanthroline and transferring it to a 100 mL flask. A small amount of concentrated hydrochloric acid (1 mL) was added in the flask and then it was filled with deionized water to the mark. The Fe^{2+} standard solutions were prepared by weighing 14.24 mg of iron(II) chloride tetrahydrate and dissolving it with 5 mL of 1:1 sulphuric acid solution in a 200 mL flask. The final concentration of Fe^{2+} was 20 μg mL^{-1}. The Fe^{2+} and Fe^{3+} standard solutions for the determination of $Fe^{2+}/(Fe^{2+} + Fe^{3+})$ ratio were prepared as follows. The Fe^{2+} standard solution was prepared by weighing 355.99 mg of iron(II) chloride tetrahydrate and dissolving it with 3 mL of concentrated hydrochloric acid in a 100 mL flask. The Fe^{3+} standard solution was prepared by weighing 483.95 mg of iron(III) chloride hexahydrate and dissolving it with 3 mL of concentrated hydrochloric acid in a 100 mL flask. The final concentrations of Fe^{2+} and Fe^{3+} were 1 mg mL^{-1}. All the solutions were prepared with deoxygenated Milli-Q water.

2.3.2 Fe^{2+} calibration curve

Solutions with different Fe^{2+} ion concentrations were prepared as follows: 0 mL, 5 mL, 10 mL, 15 mL, 20 mL, 25 mL, 30 mL of Fe^{2+} standard solution were pipetted in 100 mL flasks and in each of the 2 mL of ascorbic acid, 20 mL of acetate buffer, 10 mL of 1,10-phenanthroline were added. This resulted in the preparation of solutions of 0, 1, 2, 3, 4, 5, 6 μg mL^{-1} concentrations of Fe^{2+}. The UV-Vis absorbance of the prepared solutions was measured with a delay of 10 minutes after preparation so that Fe^{2+} was able to fully react with 1,10-phenanthroline. UV-Vis spectra were collected and the value of absorbance at 510 nm was recorded.

2.3.3 $Fe^{2+}/(Fe^{2+} + Fe^{3+})$ calibration curve

Solutions of known $Fe^{2+}/(Fe^{2+} + Fe^{3+})$ molar fractions were prepared in the range from 0.1 to 0.9 of Fe^{2+} and for each ratio the Fe^{2+} and total iron concentrations were determined. In order to prepare standard solutions with the required fractions of Fe^{2+}, 1, 3, 5, 7 and 9 mL of Fe^{2+} aliquots were mixed with 9, 7, 5, 3 and 1 mL of Fe^{3+} aliquots standard solutions, respectively. In this way, solutions with defined $Fe^{2+}/(Fe^{2+} + Fe^{3+})$ molar fractions were prepared, and each solution had a fixed total iron concentration (1 mg mL^{-1}). Considering that these concentrations are much higher than the range in which the Fe^{2+} calibration curve was constructed, the solutions were diluted approximately 200 times. For each Fe^{2+} molar fraction, two solutions were prepared: one for the determination of Fe^{2+} and one for the determination of total iron (total iron = $Fe^{2+} + Fe^{3+}$). Solutions for Fe^{2+} determination were prepared by pipetting 0.25 mL of the solutions with known $Fe^{2+}/(Fe^{2+} + Fe^{3+})$ molar fractions, adding a small amount of deoxygenated water, 10 mL of acetate buffer, 5 mL of 1,10-phenanthroline solution, and filling the remainder of the flask with deoxygenated water. Importantly, for the determination of total iron 1 mL of ascorbic acid solution was added to reduce all Fe^{3+} ions. Before adding the acetate buffer, the solution was aged for 10 minutes so that ascorbic acid could fully react with all Fe^{3+} ions. The pH values of prepared solutions were approximately 4.1 to 4.2. Absorbance was measured with a delay of 10 minutes after the addition of 1,10-phenanthroline solution. The experimental fraction of Fe^{2+} was determined by dividing the absorbance values at 510 nm for Fe^{2+} and total iron solutions according to the equation:

$$x(Fe^{2+}) = A_{510}(Fe^{2+})/A_{510}(total\ iron) \qquad (1)$$

2.3.4 1,10-phenanthroline Fe^{2+} and total iron determination in γ-irradiated samples

For the samples for spectrophotometric determination, the same procedure as in Section 2.2.1. was used, however, after irradiation, a small amount of hydrochloric acid (~2.5 vol%) was added by a syringe through the rubber septa. This was done to dissolve the formed solid products and to preserve the formed Fe^{2+} from oxidation when the flask is opened. Because the concentration of iron in the irradiated solutions is around $1.76 \cdot 10^{-2}$ M, an aliquot of 0.25 mL was pipetted to a 50 mL flask after the opening of the irradiated flask. This was done in order to dilute the iron concentration so that it is in the linear range of the tested concentrations used for

the construction of the calibration curve. The preparation of the solutions for spectrophotometric determination of Fe^{2+} and total iron proceeded according to Section 2.3.3.

3. Results

The Fe^{2+} ions form strong red-colored Fe^{2+}-1,10-phenanthroline complex with UV-Vis absorbance at 510 nm. The calibration curves for the *(i)* determination of Fe^{2+} obtained from a series of solutions of known Fe^{2+} concentrations (**Fig. S1** in Supplementary Materials), *(ii)* the calibration curve for the possible interference of Fe^{3+} in the determination of Fe^{2+} obtained from a series of solutions of known $Fe^{2+}/(Fe^{2+} + Fe^{3+})$ fractions (**Fig. S2** in Supplementary Material) and *(iii)* the possibility of the interference of polymer on the precise determination of Fe^{2+} (**Fig. S3** in Supplementary Material) were tested. The results show that the calibration curve for Fe^{2+} was highly linear in the tested range of concentrations (**Fig. S1**). The results of possible Fe^{3+} interference experiments showed that Fe^{3+} does not significantly interfere with the determination of Fe^{2+} (**Fig. S2**). In addition, it was shown that the polymer does not form a complex with 1,10-phenanthroline and does not affect the determination of Fe^{2+} (**Fig. S3**). These results are more thoroughly described in the Supplementary Materials.

The samples were synthesized by γ-irradiating colloidal suspensions of Fe^{3+} precursor in the presence of DEAE-dextran polymer in the range of doses from 5 to 130 kGy. The samples after irradiation contain different fractions of Fe^{2+}. The higher the dose, the larger the extent of reduction. However, after irradiation, these samples tend to oxidize when they come in contact with air and precise determination of the Fe^{2+} molar fractions are difficult. That is why concentrated hydrochloric acid was added to the reaction mixture immediately after irradiation through a rubber septum. At such acidic conditions, formed Fe^{2+} cannot oxidize and all of the solid precipitates are dissolved, so that they can be analyzed spectrophotometrically. For each sample, six solutions were prepared for 1,10 phenanthroline spectrophotometric determinations; three for Fe^{2+} determinations, and three for total iron determinations. A graphical representation of the course of reduction is displayed in **Fig. 1**. The standard deviation for all the measurements did not exceed 0.01 and the relative standard deviation was lower than ~1 %. The determined values of absorbance and calculated statistical parameters are shown in **Table S1** in the Supplementary Materials. **Fig. 1** shows that reduction proceeds quickly in the beginning stage of

irradiation. At a dose of 20 kGy, almost 50 % of Fe^{3+} is reduced to Fe^{2+}. After this quick initial conversion, the course of reduction slows and reaches ~100 % at 75 kGy.

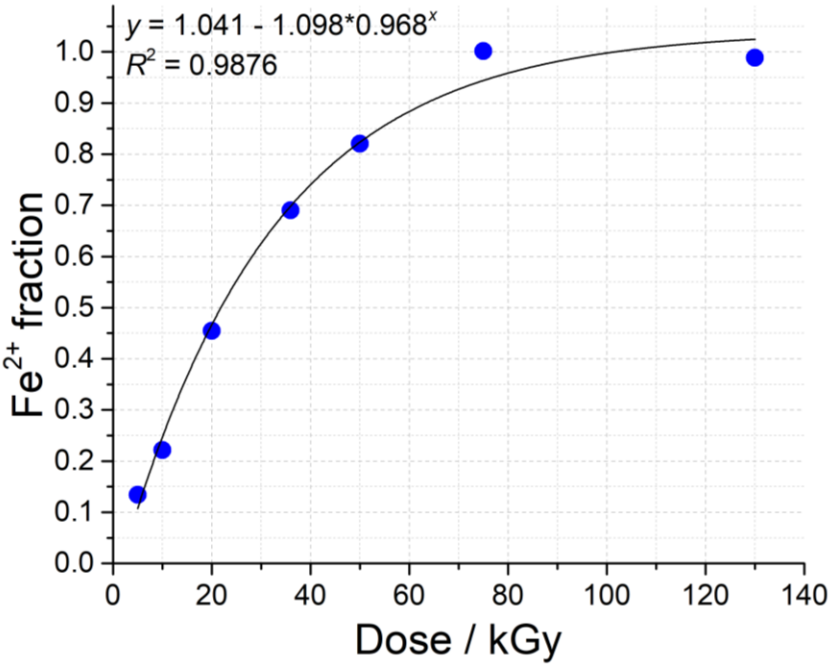

Figure 1. 1,10 phenanthroline spectrophotometric determinations of Fe^{2+} molar fractions in the γ-irradiated suspensions as a function of absorbed dose.

Fig. 2 shows XRD patterns of samples S-0 to S-130. Samples S-0, which was unirradiated, and sample S-5, consisted of 2-line ferrihydrite phase and NaCl as an impurity. The samples irradiated up to 20 kGy (samples S-10, S-14, and S-20) consisted exclusively of magnetite (Fe_3O_4). The NaCl is present as an impurity because the samples were isolated without washing. Sample S-36 consisted of magnetite, goethite (α-FeOOH), and feroxyhyte (δ-FeOOH). The samples irradiated with higher doses (50 kGy to 130 kGy) consisted of goethite, feroxyhyte, and NaCl as an impurity. The results of the line-broadening analysis are given in **Tables 1** and **2**. The Scherrer equation was used to calculate the volume-averaged domain sizes (D_v) of the dominant crystalline phases in the synthesized samples. The D_v values of magnetite were around ~8 nm (samples S-10, S-14, and S-20). The D_v values of goethite were below 5 nm, whereas the D_v values calculated from the 100 diffraction line of the δ-FeOOH were somewhat larger, ranging from 16 to 25 nm for sample S-36 to S-130, respectively. The relatively high volume

fraction of goethite (~0.60) in comparison to feroxyhyte is due to very small goethite crystallite size and isolation procedure that involved only one centrifugation. In our previous work (Jurkin et al., 2016b; Marić et al., 2019b) the synthesized feroxyhyte nanodiscs contained a minor quantity of goethite (~30 %).

Table 1. Phase composition of samples S-0 to S-130, calculated volume-averaged domain sizes of dominant phases for samples S-10 to S-120, magnetite lattice parameter for samples S-10 to S-20 and phase volume fractions for samples S-36 to S-130.

Sample	**Phase composition**	**Lattice parameter *a** / nm**	**Phase volume fraction**	**Fe^{2+} fraction[§]**
S-0	2-line ferrihydrite			-
	NaCl			
S-5	2-line ferrihydrite			0.134
	NaCl			
S-10	magnetite $Fe_{2.96}O_4$[¤]	0.8389(1)		0.222
	NaCl			
S-14	magnetite $Fe_{2.97}O_4$[¤]	0.8391(1)		0.348
	NaCl			
S-20	magnetite $Fe_{2.98}O_4$[¤]	0.8392(1)		0.455
	NaCl			
S-36	goethite		0.61	0.691
	δ-FeOOH		0.38	
	magnetite		0.01	
S-50	goethite		0.58	0.821
	δ-FeOOH		0.39	

	NaCl		0.03	
S-75	goethite		0.57	1.001
	δ-FeOOH		0.42	
	NaCl		0.01	
S-130	goethite		0.62	0.988
	δ-FeOOH		0.37	
	NaCl		0.01	

*Lattice parameter *a* refers to the magnetite lattice parameter. Therefore, the lattice parameter was only calculated for samples with high amounts of the magnetite phase.

[§]Fe^{2+} molar fractions are expressed as $Fe^{2+}/(Fe^{2+} + Fe^{3+})$ molar fractions and they are calculated according to Eq. (1).

[¤]Magnetite stoichiometry is calculated using the lattice parameter *a* according to Gorski and Scherer (2010).

Table 2. Scherrer analysis of crystal domain sizes in different *hkl* directions for goethite and δ-FeOOH phases for samples S-36 to S-130.

Sample →			**S-10**	**S-14**	**S-20**	**S-36**	**S-50**	**S-75**	**S-130**
Phase	***hkl***	**2*θ*/ °**	***D_{hkl}*/ nm**						
Magnetite	311	35.5	7.7	8.1	8.0				
Goethite	110	21.2				3.8	4.5	3.4	3.3
δ-FeOOH	100	35.1				16	17	20	25
	011	40.4				14	14	16	16
	012	53.8				10	13	16	13
	110	63.0				10	10	13	12

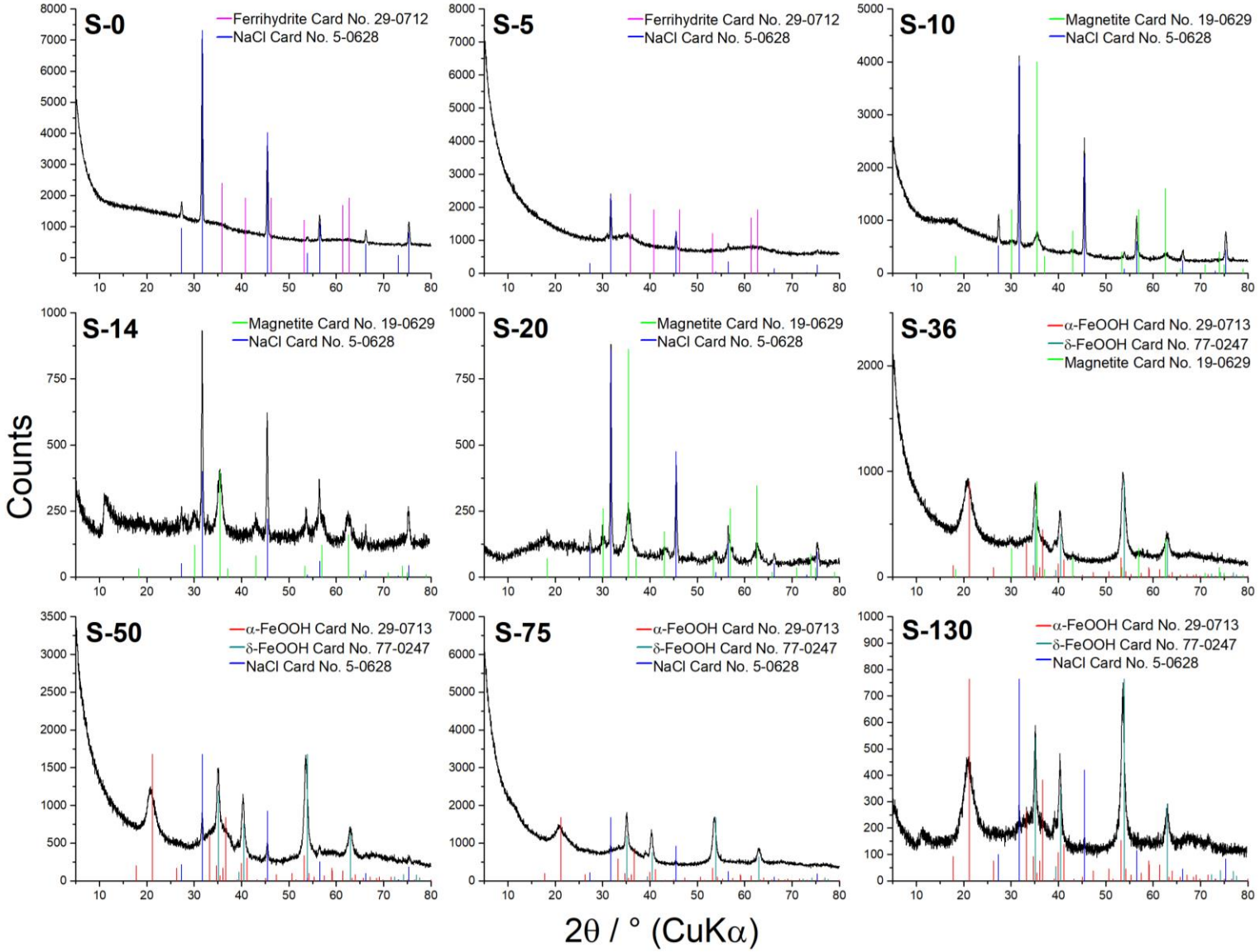

Figure 2. XRD analysis of samples S-0 to S-130.

Fig. 3 shows SEM micrographs of samples irradiated with lower doses (S-5, S-10, S-14, and S-20). Sample S-5 consisted of amorphous bulk, where no particles could be discerned. Sample S-10 consisted of the same amorphous bulk, however, larger cube-like particles can be seen, which could be attributed to the NaCl impurity. Sample S-14 consisted of 2 types of particles; larger, irregular aggregates, and small nanoparticles emerging from the bulk of the sample. Sample S-20 consisted of larger cubic particles, and smaller particles emerging from the bulk.

Fig. 4 shows SEM micrographs of samples irradiated with higher doses (S-36, S-50, S-75, and S-130). In comparison to the samples γ-irradiated with lower doses, these samples consisted of prominent and visible nanoparticles with disc-like morphology. This morphology is consistent with our previous findings (Jurkin et al., 2016b), where this disc-like morphology is attributed to δ-FeOOH. The nanodiscs aggregation differs from sample to sample. The most uniform nanodiscs are visible in sample S-50, whereas it seems that sample S-130 consists of the thinnest nanodiscs. The thickness of the nanodiscs is clearly visible in their perpendicular orientation to the viewing direction when they look like needle sticks.

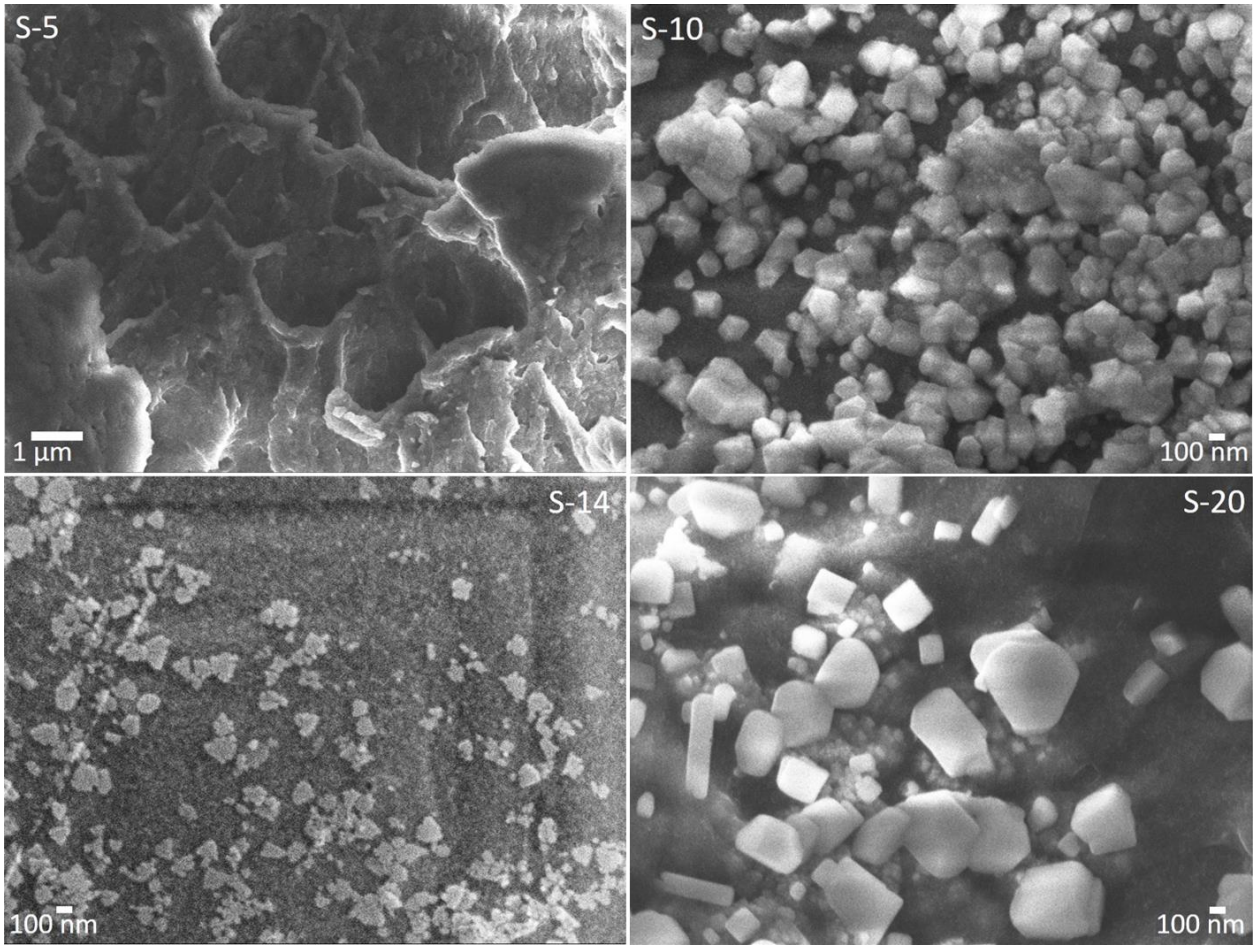

Figure 3. SEM micrographs of samples S-5 to S-20.

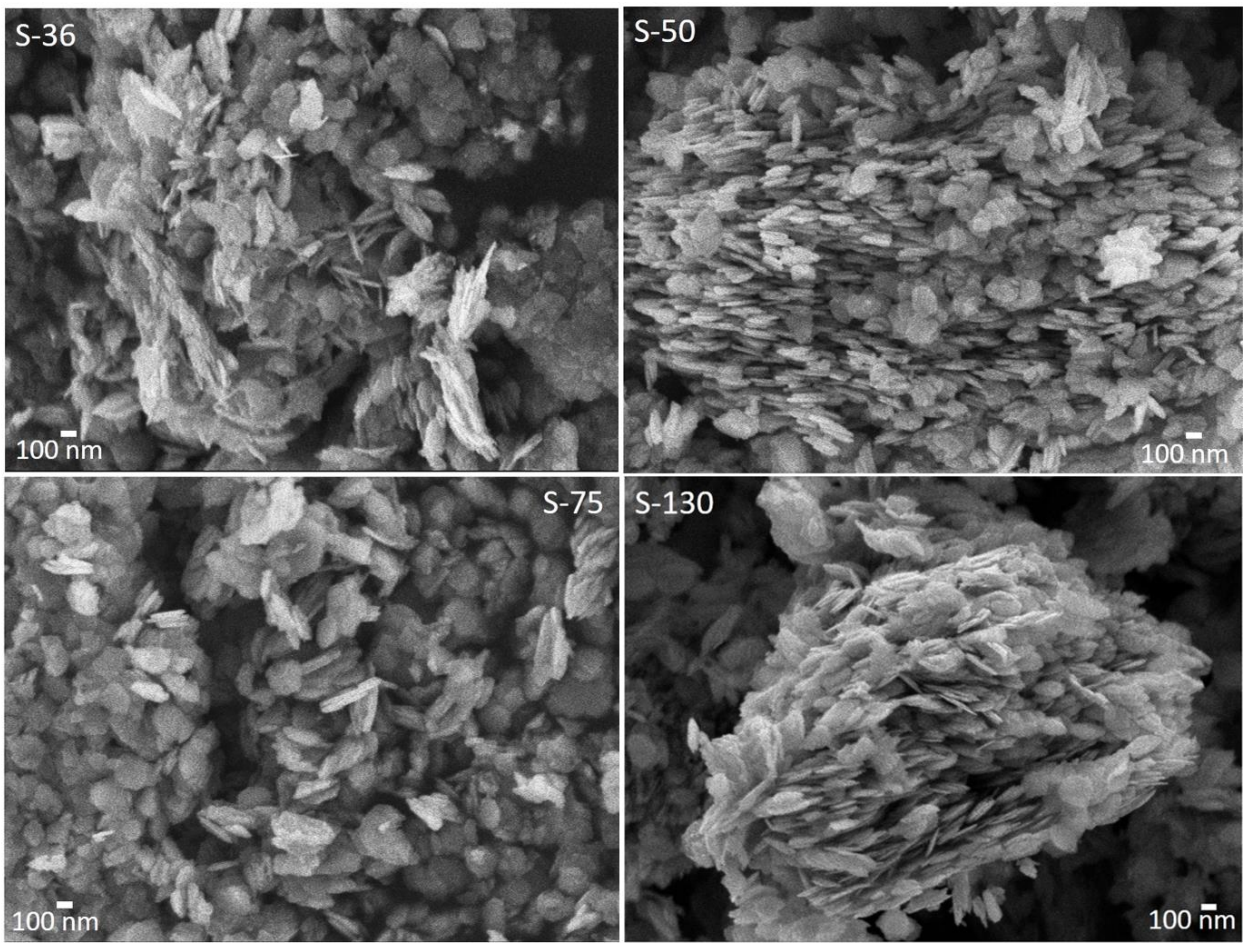

Figure 4. SEM micrographs of samples S-36 to S-130.

Fig. 5 shows the Mössbauer spectra of samples S-5 and S-75. The Mössbauer spectrum of sample S-5 is characterized by a doublet that can be ascribed to Fe(III) paramagnetic NPs or superparamagnetic NPs. The values of isomer shift (0.37 mm s^{-1}) and quadrupole splitting (0.72 mm s^{-1}) are consistent with values generally reported for trivalent iron (Gotić and Musić, 2007b). The Mössbauer spectrum of sample S-75 is characterized by a superposition of a paramagnetic and/or superparamagnetic doublet D1 and a "magnetic singlet" R, which was introduced to improve the fitting. Obviously, the synthesized samples require the detailed low-temperature and in-field Mössbauer characterizations, because of the superparamagnetic nature of synthesized nanoparticles and complex interactions between the nanoparticles of different sizes (4 nm sized α-FeOOH and 20 nm sized δ-FeOOH NPs), however these characterizations are out of scope of this study.

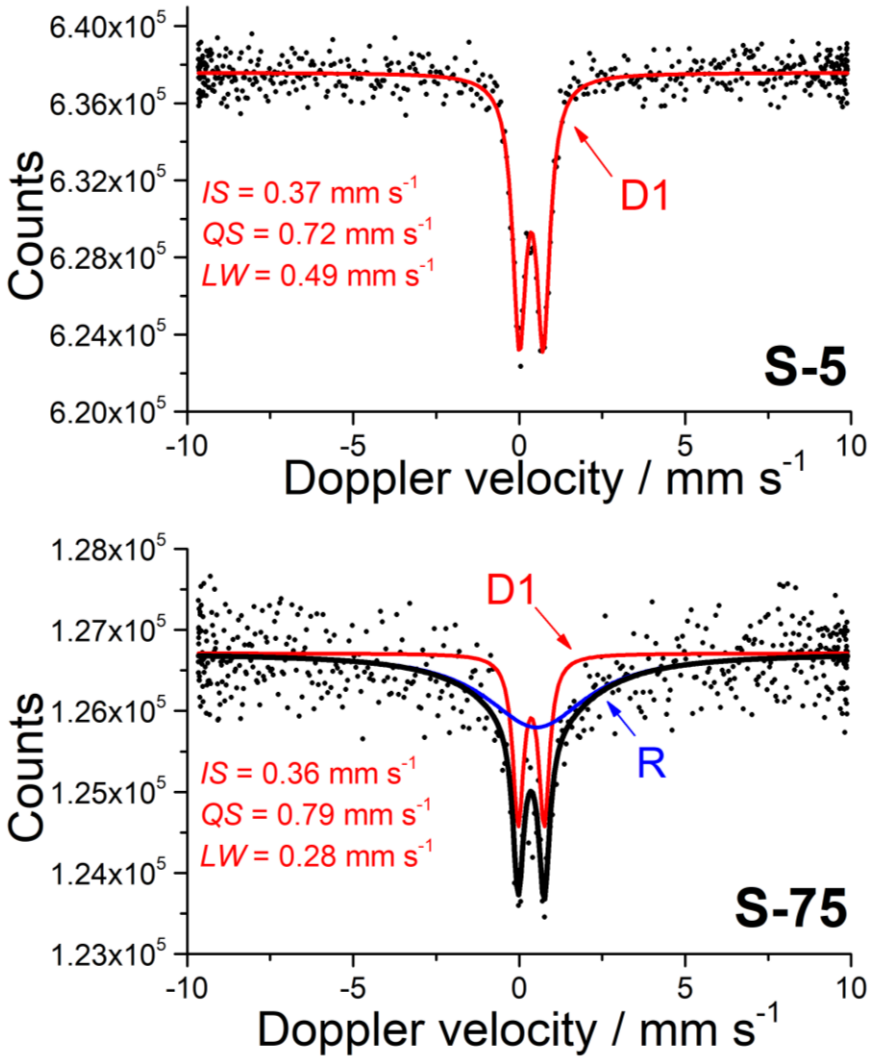

Figure 5. Room-temperature Mössbauer spectra of samples S-5 and S-75. *IS* stands for isomer shift, *QS* for quadrupole splitting and *LW* for line width.

4. Discussion

It is common that γ-irradiation is used for the synthesis of magnetite nanoparticles starting from Fe(III) precursors (Gracien et al., 2006; Wang et al., 1997; Wang and Xin, 1999), however, the quantitative determination of Fe(III) reduction and subsequently formation of Fe(II) has been hardly ever studied. In this work, we prepared the alkaline Fe(III) colloidal solutions in the presence of DEAE-dextran. The NaOH aqueous solution was used to adjust the pH to ~ 9. This precursor behaved as a colloidal solution and not as a suspension because the DEAE-dextran finely dispersed “amorphous iron(III) oxide” so that

the precursor was clear and fully transparent, red-brown (Fe^{3+}-colored) solution. The isolation of these precursor NPs was very difficult due to their very small size and high stability (centrifugation at 36,223 RCF). The XRD pattern of isolated "amorphous iron(III) oxide" precursor (sample S-0, **Fig. 2**) was consistent with 2-line ferrihydrite and NaCl crystals. The big NaCl crystals (**Fig. 3**) were present as impurities in almost all samples because the samples were not subsequently washed and centrifuged. Upon γ-irradiation, the deaerated Fe(III) alkaline precursor solution in the presence of 2-propanol and DEAE-dextran reduced to Fe(II). The degree of Fe(III) to Fe(II) reduction depends on many factors and certainly the type of polymer used is one of the key factors. The precursor solution is not stirred upon γ-irradiation and due to this reason, we use a robust cationic polymer that is able to finely disperse nanoparticles in aqueous solutions (Hanžić et al., 2018). In this way each particle has a high probability to come in contact with γ-irradiation generated reducing species. Therefore, in this work we applied the 1,10-phenanthroline spectrophotometric method in order to quantitatively measure the generation of Fe(II) upon γ-irradiation of the Fe(III) precursor. Firstly, for this purpose we ensured that there was no oxidation of radiolytically generated Fe(II) since the concentrated hydrochloric acid (~2.5 vol%) was added to the reaction mixture using a syringe through a rubber septum thus eliminating any contact of sample with oxygen. Secondly, solid Fe(II) was dissolved in this way and formed a clear and transparent aqueous solution containing all the dissolved Fe^{2+} ions that were stable against oxidation due to very low pH. Although all the Fe^{2+} ions were dissolved within clear and transparent aqueous solutions, the problem of quantitative determination of Fe^{2+} in the presence of high Fe^{3+} concentrations remained to be solved. For instance, in previous work we used permanganate titration (Marić et al., 2019a, 2019b) for Fe^{2+} quantitative determination in the same system, however, the interference of Fe^{3+} in permanganate titration method was high and it was difficult to visually determine the titration endpoint. On the other hand, the main advantage of our 1,10-phenanthroline method, which is based on the procedure given by Jiang et al. (2017), is its negligible interference of Fe^{3+} in the determination of $Fe^{2+}/(Fe^{2+}+Fe^{3+})$ ratio (**Fig. S2**). 1,10-phenanthroline results showed that γ-irradiation reduced Fe^{3+} to Fe^{2+} and that the reduction was initially very fast, but quickly slowed down and then reached 100 % reduction (**Fig. 1**). In another set of experiments, instead of preparing the sample for 1,10-phenanthroline measurements, the samples were isolated by a single centrifugation and dried in vacuum at room temperature. Only one centrifugation was performed, because in previous work we found that the oxidation state of

iron and phase composition of powder samples depended to a high extent on the isolation procedures. For instance, admixing glycerol prior to the centrifugation prevented the oxidation of Fe(II) and we managed to isolate $Fe(OH)_2$ and Green Rust I, ideal chemical formula $Fe^{II}_4Fe^{III}_2(OH)_{12}CO_3 \cdot 3H_2O$ (Marić et al., 2019a, 2019b). Herein, the isolated powder sample that was unirradiated (S-0) and sample that was irradiated at 5 kGy (S-5) were virtually amorphous, *i.e.* they consisted of 2-line ferrihydrite (**Fig. 2** and **Table 1**). The samples irradiated at doses of 10 and 20 kGy (samples S-10 and S-20) consisted of virtually stoichiometric magnetite (**Table 1**). Generally, the oxidation of Fe(II) to Fe(III) in magnetite is accompanied by a linear decrease of lattice cell parameter of stoichiometric magnetite from a = 8.396 Å to a = 8.349 Å in maghemite (γ-Fe_2O_3). The calculated lattice cell parameters of powder samples S-10 and S-20 are a = 8.389 Å and a = 8.392 Å (**Table 1**), which correspond to stoichiometries of $Fe_{2.96}O_4$ (30.1 % of Fe^{II}) and $Fe_{2.98}O_4$ (31.0 % of Fe^{II}), respectively (Gorski and Scherer, 2010). For these two samples the quantities of Fe^{2+} in the acidified solutions and quantities of Fe(II) in powder samples are in relatively good agreement (**Table 1**). However, it is known that the best stoichiometry of magnetite is achieved starting from a precursor that has exactly the ratio Fe^{2+}/Fe^{3+} = 0.5 (i.e., the stoichiometric ratio $Fe^{2+}/(Fe^{2+}+Fe^{3+})$ = 0.333). For example, in the coprecipitation synthesis, small values of Fe^{2+}/Fe^{3+} ratio lead to goethite formation, values of x = 0.3 lead to the coexistence of two phases; an oxyhydroxide phase and a nonstoichiometric magnetite, and at the value of x = 0.5, only magnetite is present, and its particles are homogeneous in size and composition (Jolivet et al., 1992). A simple asymptotic fit of the data in **Fig. 1** yielded a dose of ~14 kGy as the dose at which γ-irradiation will generate exactly 33.3 % of Fe^{2+}. However, the magnetite stoichiometry in sample S-14 did not improve ($Fe_{2.97}O_4$), even though quantitative determination of $Fe^{2+}/(Fe^{2+}+Fe^{3+})$ fraction for the S-14 sample yielded a value of ~0.35, which leads to the conclusion that γ-irradiation generated Fe^{2+} in the range of $0.25 \leq Fe^{2+}/(Fe^{2+}+Fe^{3+}) \leq 0.45$ had no decisive effect on the magnetite stoichiometry. One can argue that it is not possible that powder sample S-10 has 30.1 % of Fe(II), whereas the γ-irradiation generates only 22 % of Fe^{2+} as determined spectrophotometrically. However, the amount of 30.1% Fe^{2+} refers only to magnetite, while sample S-10 may contain some amorphous Fe(III) containing phase in addition to magnetite. The amorphous Fe(III) phase lowers the overall amount of Fe(II) in powder sample S-10 and the increased background in the XRD patterns of sample S-10 (**Fig. 2**) confirms this presumption.

When γ-irradiation generated more than 69 % of Fe^{2+} the powder samples S-36 to S-130 consisted exclusively of Fe(III), *i.e.* of δ-FeOOH nanodiscs and α-FeOOH nanoparticles about 4 nm in size. The crystallite size of formed δ-FeOOH deduced from diffraction line 100 (**Table 1**) increased from 16 nm (sample S-36) to 25 nm (sample S-130) with the increase of dose. Furthermore, the crystal anisotropy (calculated as the ratio of diffraction lines 100 and 110) of δ-FeOOH also increases from 1.6 (16 nm/10 nm) in sample S-36 to 2.1 (25 nm/12 nm,) in sample S-130.

The recipe for γ-irradiation synthesis of δ-FeOOH is first; the γ-irradiation must generate more than 69 % of Fe^{2+} at pH ≅ 9, however this is not a sufficient condition. For instance, γ-irradiation of Fe(III) precursors in the presence of dextran sulfate also generated close to 100 % of Fe^{2+}, however the formed $Fe(OH)_2$ oxidized to sulfate green rust GR(SO_4^{2-})) and then further to mixture of γ-FeOOH and α-FeOOH (Marić et al., 2019a). Additional condition for the formation of δ-FeOOH is that the formed $Fe(OH)_2$ topotactically oxidizes to carbonate green rust (GR(CO_3^{2-})), which will then further topotactically oxidize to δ-FeOOH (Jurkin et al., 2016; Marić et al., 2019b). Thus, the use of proper polymer such as DEAE-dextran is crucial for tailoring the γ-irradiation synthesis through formation of δ-FeOOH nanodiscs. On the other hand, the size and anisotropy of δ-FeOOH nanodiscs, as well as the amount of goethite as impurity, depends on the dose, dose rate, purity of chemicals, isolation procedure and many other experimental factors.

The recipe for γ-irradiation synthesis of magnetite nanoparticles is much simpler than the recipe for the formation of δ-FeOOH; the γ-irradiation should only generate about 22 to 45 % of Fe^{2+} at pH ≅ 9, and this is probably why magnetite particles are often synthesized using γ-irradiation (Ekoko et al., 2014; Gotić et al., 2009; Wang et al., 1997), while δ-FeOOH has never been synthesized using γ-irradiation until DEAE-dextran began to be used (Jurkin et al, 2016).

5. Conclusions

The 1,10-phenanthroline spectrophotometric method was used in order to quantitatively measure the Fe(III) to Fe(II) reduction upon γ-irradiation.

γ-irradiation of Fe(III) deaerated alkaline solutions in the presence of DEAE-dextran and 2-propanol reduced Fe^{3+} to Fe^{2+} completely; the reduction was initially very fast, but quickly slowed down and then reached 100 % reduction.

The quantity of Fe^{2+} in γ-irradiated suspensions and isolated solid product roughly overlap up to 45 % of Fe^{2+}, because at this range the inverse spinel structure of substoichiometric formed magnetite nanoparticles was able to capture 33.3 % of Fe^{2+}.

At more than 69 % of Fe^{2+} in suspensions the isolated solid product counterparts consist exclusively of Fe(III), namely the δ-FeOOH (feroxyhyte) nanodiscs and α-FeOOH (goethite) of about 4 nm in size were formed.

The absorbed dose increased the crystal size and crystal aspect ratio of δ-FeOOH nanodiscs.

The absorbed dose had no influence on the stoichiometry of the formed magnetite NPs in the range from 10 to 20 kGy, even though Fe^{2+} molar fraction varies from ~0.22 to ~0.45.

Acknowledgments

This work was financially supported by the Croatian Science Foundation under the project UIP-2017-05-7337 “The impact of polymers on the radiolytic synthesis of magnetic nanoparticles” (POLRADNANOP).

References

Ekoko, G.B., Lobo, J.K.-K., Mvele, O.M., Muswema, J.L., Yamambe, J.-F.S., Mangwala, P.K., 2014. Gamma irradiation inducing the synthesis of magnetic Fe_3O_4 nanorod particles in alkaline medium. Int. J. Mater. Sci. Appl. 3, 339-343. https://doi.org/10.11648/j.ijmsa.20140306.20

Gorski, C.A., Scherer, M.M., 2010. Determination of nanoparticulate magnetite stoichiometry by Mossbauer spectroscopy, acidic dissolution, and powder X-ray diffraction: A critical review. Am. Mineral. 95, 1017–1026. https://doi.org/10.2138/am.2010.3435

Gotić, M., Jurkin, T., Musić, S., 2009. From iron(III) precursor to magnetite and vice versa. Mater. Res. Bull. 44, 2014–2021. https://doi.org/10.1016/j.materresbull.2009.06.002

Gotić, M., Jurkin, T., Musić, S., 2007a. Factors that may influence the micro-emulsion synthesis of nanosize magnetite particles. Colloid Polym. Sci. 285, 793–800. https://doi.org/10.1007/s00396-006-1624-2

Gotić, M., Musić, S., 2007b. Mössbauer, FT-IR and FE SEM investigation of iron oxides precipitated from $FeSO_4$ solutions. J. Mol. Struct. 834–836, 445–453. https://doi.org/10.1016/j.molstruc.2006.10.059

Gotić, M., Popović, S., Musić, S., 1994. Formation and characterization of δ-FeOOH. Mater. Lett. 21, 289-295. https://doi.org/10.1016/0167-577X(94)90192-9

Gracien, E.B., Ruimin, Z., LiHui, X., Kanza, L.K., Lopaka, I., 2006. Effects of pH on the morphology of iron oxides synthesized under gamma-irradiation. J. Radioanal. Nucl. Chem. 270, 473–478. https://doi.org/10.1007/s10967-006-0374-4

Gupta, A.K., Gupta, M., 2005. Synthesis and surface engineering of iron oxide nanoparticles for biomedical applications. Biomaterials 26, 3995–4021. https://doi.org/10.1016/j.biomaterials.2004.10.012

Hanžić, N., Horvat, A., Bibić, J., Unfried, K., Jurkin, T., Dražić, G., Marijanović, I., Slade, N., Gotić, M., 2018. Syntheses of gold nanoparticles and their impact on the cell cycle in breast cancer cells subjected to megavoltage X-ray irradiation. Mat. Sci. Eng. C-Biomim. 91, 486-495. https://doi.org/10.1016/j.msec.2018.05.066.

Hartmann, J., Asch, F., 2018. Micro-method to determine iron concentrations in plant tissues using 2,2′ bipyridine. J. Plant Nutr. Soil Sci. 181, 357–363. https://doi.org/10.1002/jpln.201700433

Jiang, C., Yang, S., Gan, N., Pan, H., Liu, H., 2017. A method for determination of $[Fe^{3+}]/[Fe^{2+}]$ ratio in superparamagnetic iron oxide. J. Magn. Magn. Mater. 439, 126–134. https://doi.org/10.1016/j.jmmm.2017.04.073

Jolivet, J.P., Belleville, P., Tronc, É., Livage, J., 1992. Influence of Fe(II) on the formation of the spinel iron oxide in alkaline medium. Clays Clay Miner. 40, 531–539. https://doi.org/10.1346/CCMN.1992.0400506

Jurkin, T., Gotić, M., Štefanić, G., Pucić, I., 2016a. Gamma-irradiation synthesis of iron oxide nanoparticles in the presence of PEO, PVP or CTAB. Radiat. Phys. Chem. 124, 75–83. https://doi.org/10.1016/j.radphyschem.2015.11.019

Jurkin, T., Štefanić, G., Dražić, G., Gotić, M., 2016b. Synthesis route to δ-FeOOH nanodiscs. Mater. Lett. 173, 55–59. https://doi.org/https://doi.org/10.1016/j.matlet.2016.03.009

Koch, C.B., Oxborrow, C.A., Mørup, S., Madsen, M.B., Quinn, A.J., Coey, J.M.D., 1995. Magnetic properties of feroxyhyte (δ-FeOOH). Phys. Chem. Miner. 22, 333–341. https://doi.org/10.1007/BF00202774

Laurent, S., Forge, D., Port, M., Roch, A., Robic, C., Vander Elst, L., Muller, R.N., 2008. Magnetic iron oxide nanoparticles: synthesis, stabilization, vectorization, physicochemical characterizations, and biological applications. Chem. Rev. 108, 2064–2110. https://doi.org/10.1021/cr068445e

Lutterotti, L., Bortolotti, M., Ischia, G., Lonardelli, I., Wenk, H.-R., 2007. Rietveld texture analysis from diffraction images. Z. Kristallogr., Suppl. 26, 125-130.

Marić, I., Štefanić, G., Gotić, M., Jurkin, T., 2019a. The impact of dextran sulfate on the radiolytic synthesis of magnetic iron oxide nanoparticles. J. Mol. Struct. 1183, 126–136. https://doi.org/10.1016/j.molstruc.2019.01.075

Marić, I., Dražić, G., Štefanić, G., Zadro, K., Gotić, M., Jurkin, T., 2019b. Characterization of radiolytically synthesized feroxyhyte and oxidized magnetite nanoparticles. Mater. Charact, *In press*, https://doi.org/10.1016/j.matchar.2019.110038

Massart, R., 1981. Preparation of aqueous magnetic liquids in alkaline and acidic media. IEEE Trans. Magn. 17, 1247–1248. https://doi.org/10.1109/TMAG.1981.1061188

Pernet, M., Obradors, X., Fontcuberta, J., Joubert, J.C., Tejada, J., 1984. Magnetic structure and supermagnetic properties of δ-FeOOH. IEEE Trans. Magn. 20, 1524–1526. https://doi.org/10.1109/TMAG.1984.1063311

Pollard, R.J., Pankhurst, Q.A., 1991. Ferrimagnetism in fine feroxyhite particles. J. Magn. Magn. Mater. 99, L39–L44. https://doi.org/10.1016/0304-8853(91)90045-C

Qu, W., Zhou, C.Y., Liu, S., 2014. Synchronous determination of copper, iron, nickel, lead, cadmium and chromium in electroplating wastewater by ICP-AES. Adv. Mater. Res. 1033–1034, 558–562. https://doi.org/10.4028/www.scientific.net/AMR.1033-1034.558

Seeger, T.S., Rosa, F.C., Bizzi, C.A., Dressler, V.L., Flores, E.M.M., Duarte, F.A., 2015. Feasibility of dispersive liquid–liquid microextraction for extraction and preconcentration of Cu and Fe in red and white wine and determination by flame atomic absorption spectrometry. Spectrochim. Acta Part B At. Spectrosc. 105, 136–140. https://doi.org/10.1016/j.sab.2014.11.002

Sestu, M., Carta, D., Casula, M.F., Corrias, A., Navarra, G., 2015. Novel interpretation of the mean structure of feroxyhyte. J. Solid State Chem. 225, 256–260. https://doi.org/10.1016/j.jssc.2015.01.003

Sutherland, T.I., Sparks, C.J., Joseph, J.M., Wang, Z., Whitaker, G., Sham, T.K., Wren, J.C., 2016. Effect of ferrous ion concentration on the kinetics of radiation-induced iron-oxide nanoparticle formation and growth. Phys. Chem. Chem. Phys. 19, 695–708. https://doi.org/10.1039/c6cp05456k

Tamura, H., Goto, K., Yotsuyanagi, T., Nagayama, M., 1974. Spectrophotometric determination of iron(II) with 1,10-phenanthroline in the presence of large amounts of iron(III). Talanta 21, 314–318. https://doi.org/10.1016/0039-9140(74)80012-3

Thomas, L.A., Dekker, L., Kallumadil, M., Southern, P., Wilson, M., Nair, S.P., Pankhurst, Q.A., Parkin, I.P., 2009. Carboxylic acid-stabilised iron oxide nanoparticles for use in magnetic hyperthermia. J. Mater. Chem. 19, 6529. https://doi.org/10.1039/b908187a

Toby, B.H., 2005. CMPR – a powder diffraction toolkit. J. Appl. Crystallogr. 38, 1040–1041. https://doi.org/10.1107/S0021889805030232

Viollier, E., Inglett, P.W., Hunter, K., Roychoudhury, A.N., Van Cappellen, P., 2000. The ferrozine method revisited: Fe(II)/Fe(III) determination in natural waters. Appl. Geochemistry 15, 785–790. https://doi.org/10.1016/S0883-2927(99)00097-9

Wang, S., Xin, H., 1999. The γ-irradiation-induced chemical change from β-FeOOH to Fe_3O_4. Radiat. Phys. Chem. 56, 567–572. https://doi.org/10.1016/S0969-

806X(99)00319-9

Wang, S., Xin, H., Qian, Y., 1997. Preparation of nanocrystalline Fe_3O_4 by γ-ray radiation. Mater. Lett. 33, 113–116. https://doi.org/10.1016/S0167-577X(97)00077-3

Xu, P., Zeng, G.M., Huang, D.L., Feng, C.L., Hu, S., Zhao, M.H., Lai, C., Wei, Z., Huang, C., Xie, G.X., Liu, Z.F., 2012. Use of iron oxide nanomaterials in wastewater treatment: A review. Sci. Total Environ. 424, 1–10. https://doi.org/10.1016/j.scitotenv.2012.02.023

Yakabuskie, P.A., Joseph, J.M., Keech, P., Botton, G.A., Guzonas, D., Wren, J.C., 2011. Iron oxyhydroxide colloid formation by gamma-radiolysis. Phys. Chem. Chem. Phys. 13, 7198. https://doi.org/10.1039/c1cp20084d

Supplementary Materials

γ-irradiation generated ferrous ions affect the formation of magnetite and feroxyhyte

I. Marić[1], M. Gotić[2,3], G. Štefanić[2,3], A. Pustak[1], T. Jurkin[1,*]

[1]*Radiation Chemistry and Dosimetry Laboratory, Ruđer Bošković Institute, Bijenička c. 54,10000 Zagreb, Croatia*
[2]*Center of Excellence for Advanced Materials and Sensing Devices, Ruđer Bošković Institute, Bijenička c. 54, 10000 Zagreb, Croatia*
[3]*Laboratory for Molecular Physics and Synthesis of New Materials, Division of Materials Physics, Ruđer Bošković Institute, Bijenička c. 54, 10000 Zagreb, Croatia*

*Corresponding author: Dr. Tanja Jurkin, Radiation Chemistry and Dosimetry Laboratory,Ruđer Bošković Institute, Bijenička 54, 10000 Zagreb, Croatia, Phone: +385 1 4571 255, *E-mail address*: tjurkin@irb.hr

Table of Contents

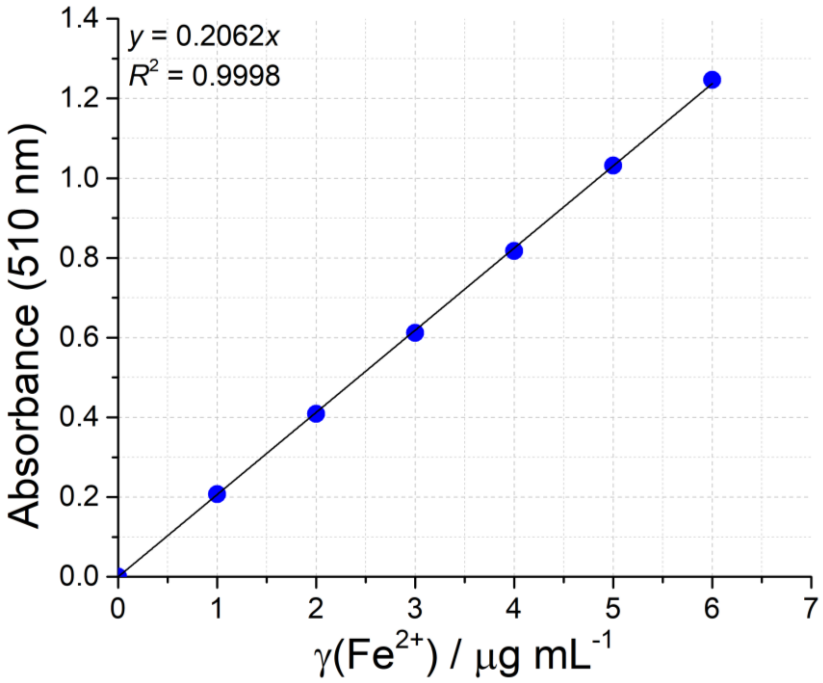

Figure S1. UV-Vis absorbance at 510 nm in dependence of Fe^{2+} mass concentrations.

UV-Vis absorbance at 510 nm is due to the formed strong red-colored Fe^{2+}-1,10 phenanthroline complex. The calibration curve and corresponding linear regression equation and R^2 (coefficient of determination) value are given. In the tested range of mass concentrations from 0 to 6 μg mL^{-1} of Fe^{2+}, the dependence of absorbance on $\gamma(Fe^{2+})$ is highly linear (R^2 = 0.9998). The equation $y = 0.2062x$ was modeled according to Beer-Lambert equation ($A = ab\gamma$) where y corresponds to absorbance, the slope (0.2062) corresponds to the product of beam path length and absorption coefficient, and x represents the mass concentration. The equation was used to calculate unknown Fe^{2+} concentrations. Considering that the dependence is linear in the tested range, the synthesized sample solutions were diluted so that their Fe^{2+} concentrations are somewhere in this range (~5 μg mL^{-1}).

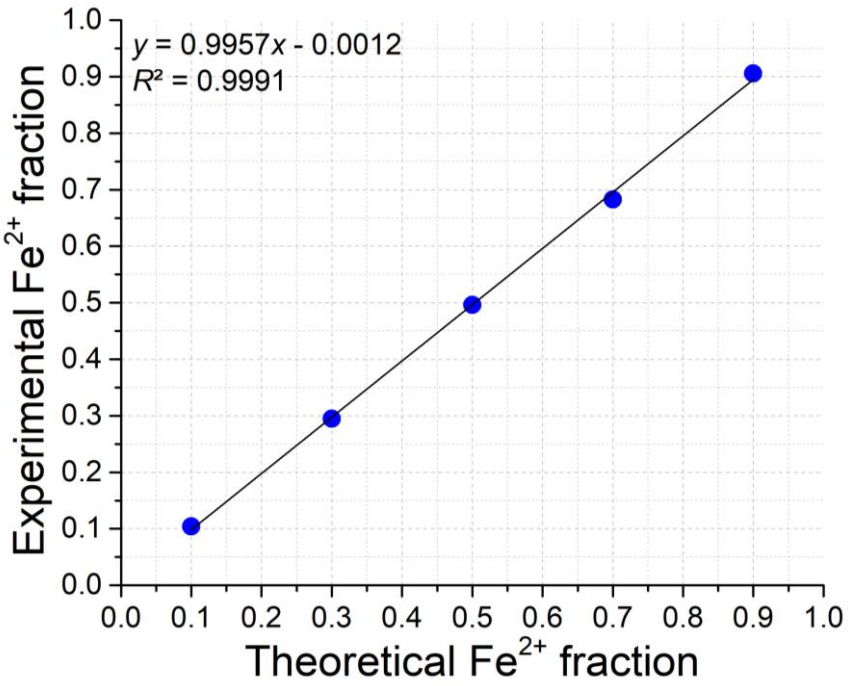

Figure S2. $Fe^{2+}/(Fe^{2+} + Fe^{3+})$ fraction values experimentally determined as a function of theoretical molar fractions.

A calibration curve for the $Fe^{2+}/(Fe^{2+} + Fe^{3+})$ molar fractions was constructed to check if Fe^{3+} ions interfere in the determination of Fe^{2+} as observed in some papers (Tamura et al., 1974; Jiang et al. 2017). The theoretical and experimental values of the molar fractions are highly correlated, as expected. The linear equation obtained by fitting the data shows that the experimental values of the fraction are virtually identical to the calculated values of the $Fe^{2+}/(Fe^{2+} + Fe^{3+})$ molar fractions. Therefore, it can be concluded that Fe^{3+} ions do not interfere with the determination of Fe^{2+} and that the experimentally determined values of the molar fractions do not need to be corrected.

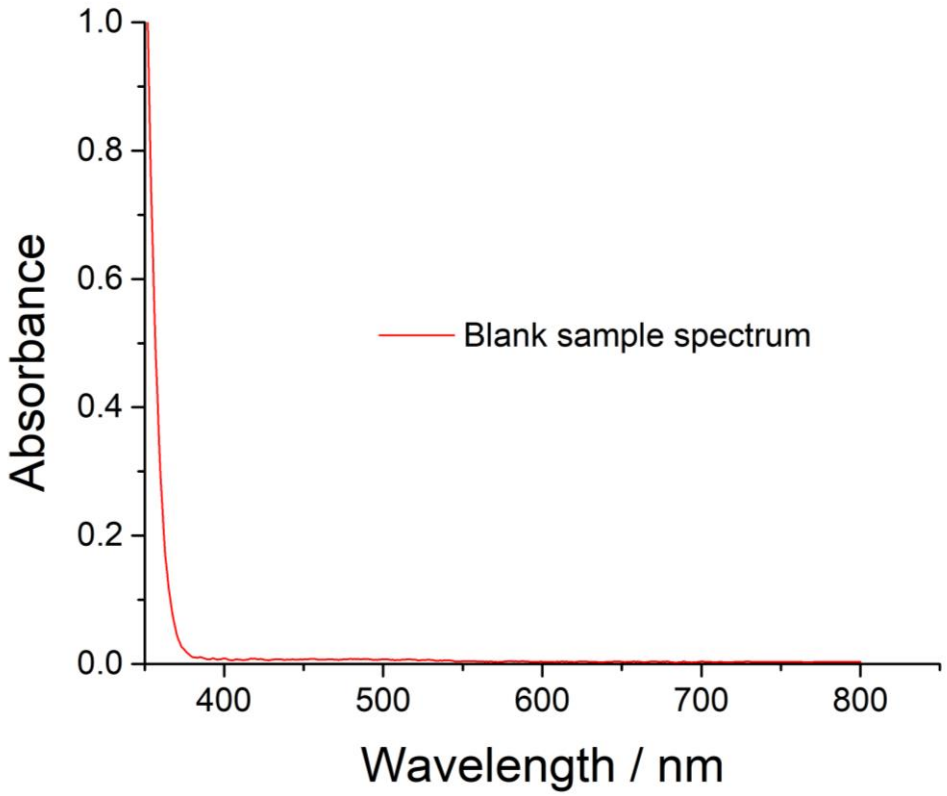

Figure S3. UV-Vis spectrum of the "blank" sample (γ-irradiated to 36 kGy of aqueous solution in the presence of DEAE dextran, but without the addition of iron(III)).

The "blank" sample was prepared following the exact same procedure as outlined in Sections 2.2.1. and 2.3.4. of the Manuscript, in order to determine whether the polymer, present in a significant amount in radiolytically synthesized samples, affects the absorbance of the Fe^{2+}-phenanthroline complex, or whether the polymer somehow reacts with 1,10-phenanthroline, the absorbance of the blank at 510 nm is negligible (~0.005), therefore, it can be concluded that the polymer has no interaction with 1,10-phenanthroline and that it does not interfere with the determination of iron.

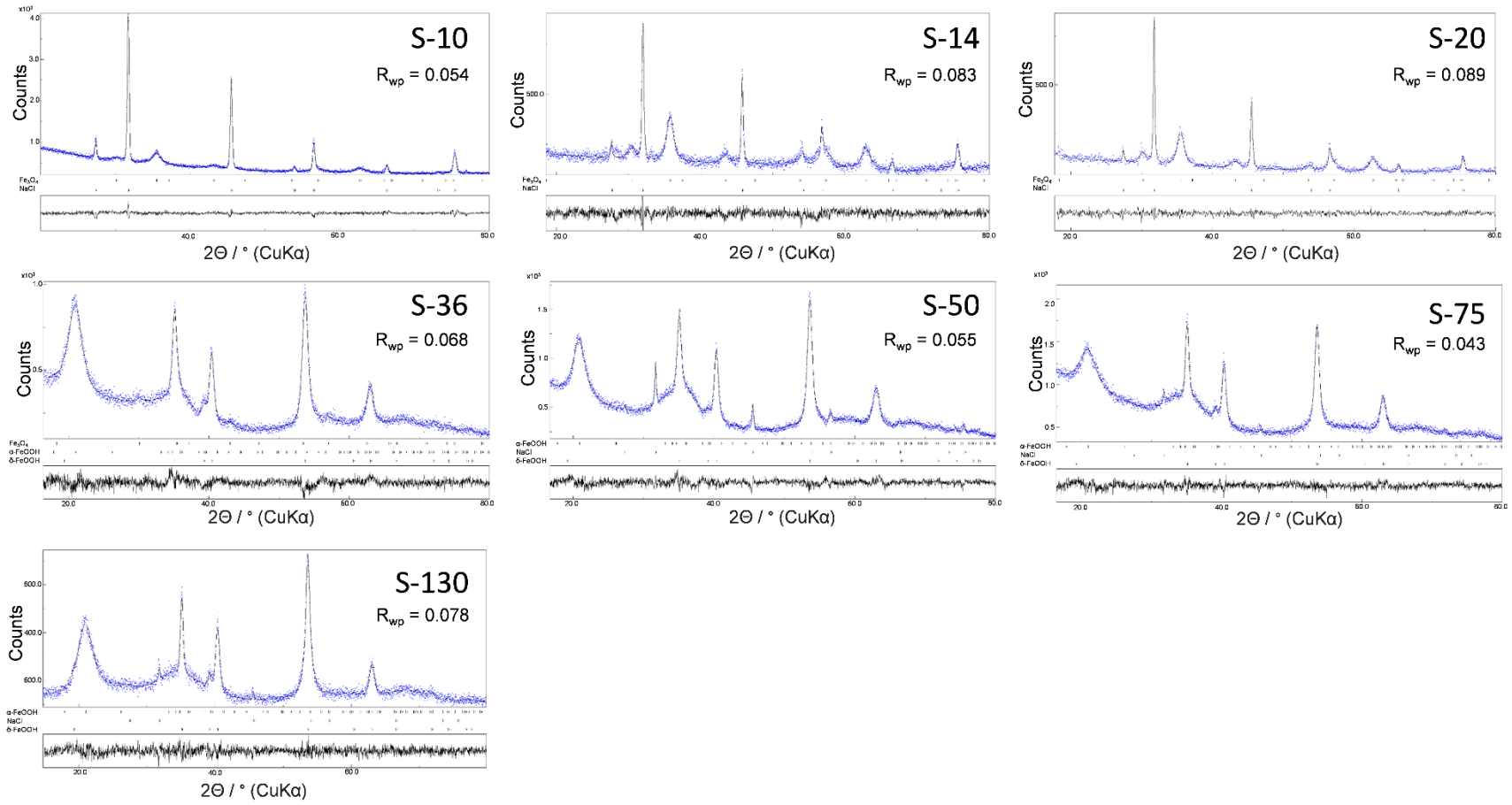

Figure S4. Rietveld refinement results of samples S-10 to S-130 with corresponding R_{wp} values. The results of calculated volume fraction for each phase are given in Table 1 in the manuscript.

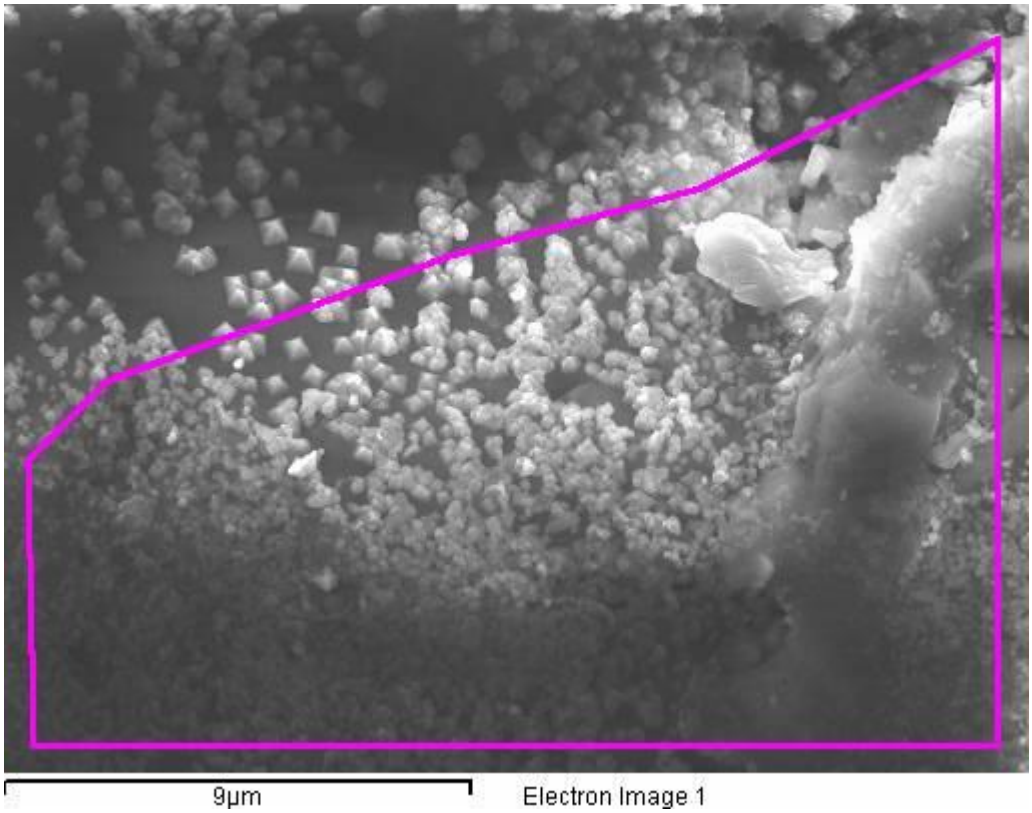

Element	Weight%	Atomic%
C K	43.15	57.01
O K	29.43	29.20
Na K	8.65	5.97
Si K	1.87	1.05
Cl K	12.00	5.37
Fe K	4.90	1.39
Totals	100.00	

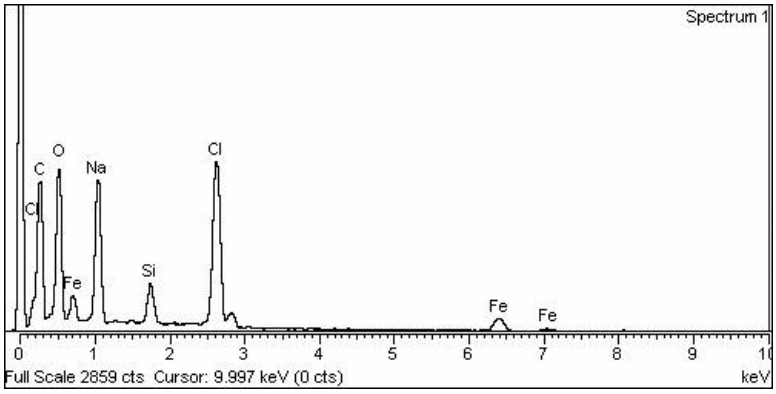

Figure S5. Scanning Electron Microscopy (SEM) image and corresponding Energy Dispersive X-ray Spectroscopy (EDS) results (tabular and graphical presentations) of the S-10 sample.The analysis was performed on the area bordered by purple color. The amount of carbon is very high due to the presence of DEAE dextran polymer and because the sample is placed on a graphite tape. High amount of oxygen is due to the DEAE dextran polymer and the formed magnetite. High concentration of Na (5.97 %) and Cl (5.37 %) and approximate stoichiometry of 1:1 indicate that these large crystallites are NaCl crystals. This conclusion is corroborated by the fact that NaCl phase diffraction maxima had very small values of FWHM (full width at half maximum) which indicates that these crystallites are very large. A small amount of Si is likely due to the dissolution of the glassware used in the synthesis (pH of the suspensions before irradiation was ~9).

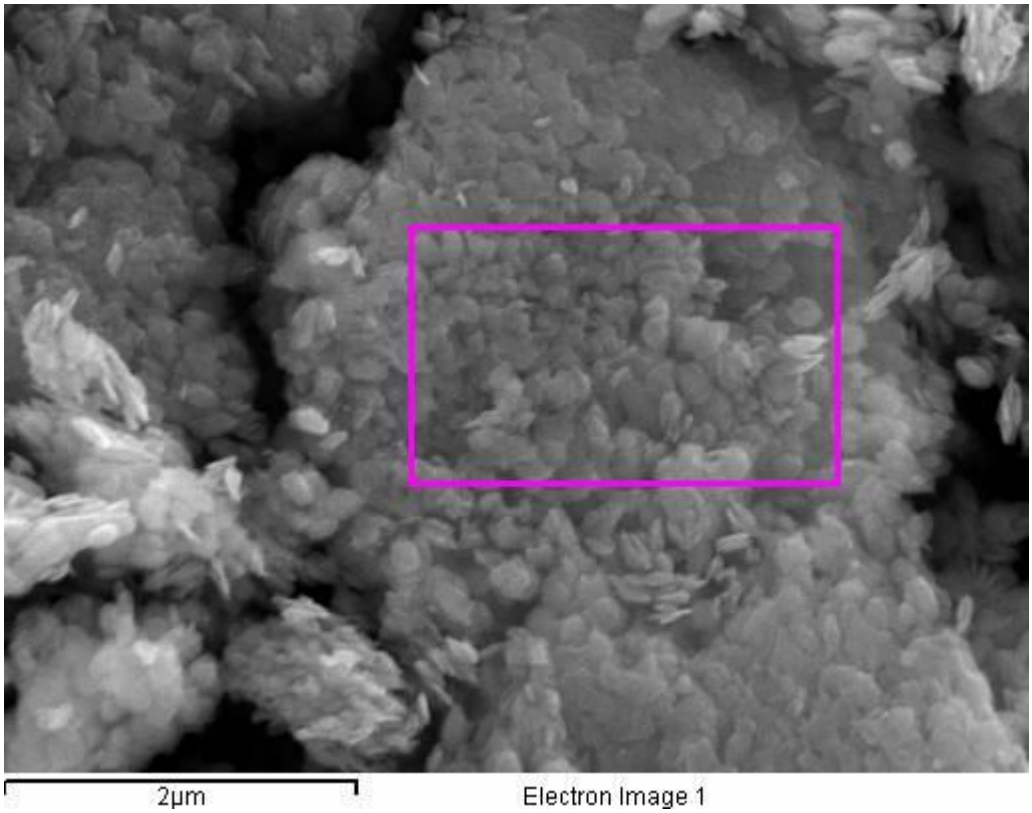

Element	Weight%	Atomic%
C K	4.16	9.45
O K	35.48	60.54
Na K	0.36	0.42
Cl K	0.88	0.68
Fe K	59.13	28.91
Totals	100.00	

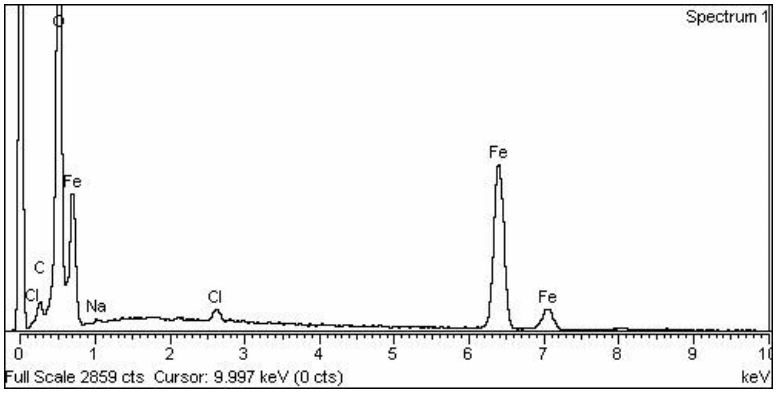

Figure S6. Scanning Electron Microscopy (SEM) image and corresponding Energy Dispersive X-ray Spectroscopy (EDS) results (tabular and graphical presentations) of the S-130 sample.The analysis was performed on the area bordered by purple color. The oxygen/iron ratio is approximately 2.1, which is in excellent agreement to XRD analysis of this sample. XRD analysis showed that this sample consists of iron oxyhydroxide phases (α-FeOOH and δ-FeOOH) with oxygen/iron ratio of 2. The excess of oxygen in this sample can be attributed to DEAE dextran polymer or to radiolytic products of the polymer. Furthermore, the presence of Na and Cl is also consistent with XRD analysis of this sample which identified NaCl phase as present in the sample.

Table S1. Results of the 1,10 phenanthroline spectrophotometric determination of Fe^{2+} for three repeat measurements, values of Fe^{2+} fraction and calculations of basic statistical parameters.

		Fe^{2+} determination			total iron determination			Fe^{2+} molar fractions*			basic statistical parameters			
Sample	Dose / kGy	A_1	A_2	A_3	A_1	A_2	A_3	F_1	F_2	F_3	F_{avg}¤	*SD*	*RSD* / %	Relative error§ / %
S-5	5	0.1232	0.1226	0.1219	0.9155	0.9108	0.9116	0.1346	0.1346	0.1337	0.1343	0.000502	0.37	2.38
S-10	10	0.2115	0.2119	0.2148	0.9547	0.9547	0.9672	0.2215	0.2220	0.2221	0.2219	0.000287	0.13	2.59
S-20	20	0.4374	0.4379	0.4376	0.9583	0.9649	0.9639	0.4564	0.4538	0.4540	0.4548	0.001459	0.32	2.86
S-36	36	0.6311	0.6309	0.6333	0.9161	0.9139	0.9143	0.6889	0.6903	0.6927	0.6906	0.001898	0.27	0.04
S-50	50	0.8000	0.8013	0.8014	0.9783	0.9743	0.9750	0.8177	0.8224	0.8219	0.8207	0.002579	0.31	4.37
S-75	75	0.9499	0.9443	0.9430	0.9440	0.9428	0.9465	1.0063	1.0016	0.9963	1.0014	0.004977	0.50	1.02
S-130	130	0.9084	0.9144	0.9159	0.9214	0.9195	0.9303	0.9859	0.9945	0.9845	0.9883	0.005383	0.54	1.24

*Fe^{2+} molar fractions are expressed as $Fe^{2+}/(Fe^{2+} + Fe^{3+})$ molar fractions. Each *F* value is the result of dividing the corresponding *A* value for Fe^{2+} determination by the corresponding *A* value for total iron determination.

¤Average value of three *F* values.

§The relative errors % refer to the relative error in the determination of total iron in the system. This is calculated as $(|c_t-c_s|/c_t)\cdot 100$ %, where c_t is the starting concentration of iron in the system and c_s is the spectrophotometrically determined concentration of iron.

References

Jiang, C., Yang, S., Gan, N., Pan, H., Liu, H., 2017. A method for determination of [Fe^{3+}]/[Fe^{2+}] ratio in superparamagnetic iron oxide. J. Magn. Magn. Mater. 439, 126–134. https://doi.org/10.1016/j.jmmm.2017.04.073

Tamura, H., Goto, K., Yotsuyanagi, T., Nagayama, M., 1974. Spectrophotometric determination of iron(II) with 1,10-phenanthroline in the presence of large amounts of iron(III). Talanta 21, 314–318. https://doi.org/10.1016/0039-9140(74)80012-3